Journal of Power Sources 371 (2017) 225–237

Contents lists available at ScienceDirect

Journal of Power Sources

journal homepage: www.elsevier.com/locate/jpowsour

Solid oxide fuel cell short stack performance testing - Part A: Experimental analysis and μ-combined heat and power unit comparison

L. Mastropasqua[a,b,*], S. Campanari[a], J. Brouwer[b]

[a] Politecnico di Milano, Department of Energy, Via Lambruschini 4, 20156 Milan, Italy
[b] National Fuel Cell Research Center, University of California, Irvine, CA 92697-3550, United States

HIGHLIGHTS

- Assessment of thermodynamic and environmental performances of a SOFC short-stack.
- Short-stack dynamic shall be considered in polarisation curve testing.
- Short-stacks give a good representation of full-scale commercial units.
- NO_x emissions result extremely limited from the fuel cell stack.

ARTICLE INFO

Keywords:
Solid oxide fuel cell
Short stack
Micro-CHP
Polarisation curve
Emission
Experimental

ABSTRACT

The need to experimentally understand the detailed performance of SOFC stacks under operating conditions typical of commercial SOFC systems has prompted this two-part study. The steady state performance of a 6-cell short stack of yttria (Y_2O_3) stabilised zirconia (YSZ) with Ni/YSZ anodes and composite Sr-doped lanthanum manganite ($LaMnO_3$, LSM)/YSZ cathodes is experimentally evaluated. In Part A, the stack characterisation is carried out by means of sensitivity analyses on the fuel utilisation factor and the steam-to-carbon ratio. Electrical and environmental performances are assessed and the results are compared with a commercial full-scale micro-CHP system, which comprises the same cells.

The results show that the measured temperature dynamics of the short stack in a test stand environment are on the order of many minutes; therefore, one cannot neglect temperature dynamics for a precise measurement of the steady state polarisation behaviour. The overall polarisation performance is comparable to that of the full stack employed in the micro-CHP system, confirming the good representation that short-stack analyses can give of the entire SOFC module. The environmental performance is measured verifying the negligible values of NO emissions (< 10 ppb) across the whole polarisation curve.

1. Introduction

Within the past twenty years, high temperature fuel cells (i.e., solid oxide fuel cells, SOFC, and molten carbonate fuel cells, MCFC) have gained the attention of most of the energy community and the industrial sector for their potential in both high efficiency Distributed Generation (DG) applications and in future larger power generation applications with low or zero carbon emissions. Their high efficiency and low-carbon characteristics make them a necessary component of most energy future scenarios that target the reduction of anthropogenic carbon emissions [1] and air quality improvement [2].

In particular, Solid Oxide Fuel Cells (SOFC) are experiencing important successes due to many publicly funded projects, especially in Europe [3–7] and Japan [8] for micro-CHP applications and in the USA for low carbon coal plants and H_2 energy [9–11]. Moreover, the commercialisation of SOFC systems is ongoing thanks to the involvement of numerous industrial actors including, among others, Fuel Cell Energy (USA) [12,13], Bloom Energy (USA) [14], Solid Power (Italy) [15], Elcogen (Finland) [16] and Ceres Power (UK) [17]. Many of these companies have already demonstrated the potential of SOFC systems to reach 60% + electric efficiencies even at the very small size class of a few kW_{el} [18–23]. Other actors are also working on their process integration with many R & D efforts on hybrid SOFC systems, such as GE (USA) [24] and LG Fuel Cell Systems [25].

Based on this background, it is important to understand SOFC stack electrochemical performance under operating conditions relevant to

* Corresponding author. Politecnico di Milano, Department of Energy, Via Lambruschini 4, 20156 Milan, Italy.
E-mail address: luca.mastropasqua@polimi.it (L. Mastropasqua).

http://dx.doi.org/10.1016/j.jpowsour.2017.10.028
Received 1 June 2017; Received in revised form 7 October 2017; Accepted 10 October 2017
Available online 16 October 2017
0378-7753/

Nomenclature

Acronyms

SOFC	Solid Oxide Fuel Cell
DIR	Direct Internal Reforming
DG	Distributed Generation
SMR	Steam Methane Reforming
WGS	Water Gas Shift
CCS	Carbon Capture and Storage
LHV	Lower Heating Value

List of symbols

$\dot{W}_{el}$ $[kW]$	Electric Power Output
U_f [%]	Fuel Utilisation factor
U_{ox} [%]	Oxidant Utilisation factor
S/C [−]	Steam-to-Carbon Ratio
η_I [%]	First law efficiency
η_{el} [%]	Electric efficiency
$\dot{Q}$ $[MW]$	Thermal power
P $[Pa]$	Pressure
h_s $[kJ\ kg^{-1}]$	Static enthalpy
$\dot{m}$ $[kg\ s^{-1}]$	Mass flow rate
$\dot{n}$ $[mol\ s^{-1}]$	Molar flow rate
T_{ai} [°C]	Temperature Air Inlet
T_{ao} [°C]	Temperature Air Outlet
T_{fi} [°C]	Temperature Fuel Inlet
T_{fo} [°C]	Temperature Fuel Outlet
TT [°C]	Temperature Top Stack
TB [°C]	Temperature Bottom Stack

commercial systems operation. It is thus required to test the thermodynamic and environmental performance of SOFC-based systems in order to guide the technology roadmaps and support the successful market deployment of these systems.

The need to experimentally understand the detailed performance of commercial SOFC stacks, has prompted this two-part study. Part A presented here provides a description of the test stand and the experimental methodology, aiming at the thermodynamic and environmental characterisation of the system and its comparison with a commercial micro-CHP unit. On the other hand, Part B of this study is focused on stack performance assessment in operating conditions typical of CCS operation, including conditions with anode recycle typical of multi-MW centralised power generation systems. The work is carried out at the National Fuel Cell Research Center (NFCRC) at the University of California, Irvine using the Short Stack Test Bench (SSTB) manufactured by SOLIDPower S.p.a. (Italy).

The objectives of this paper are summarised as follows:

- Characterise the steady state and dynamic response of a short SOFC stack for various operating conditions and power ranges
- Perform a sensitivity analysis on the main operating parameters in order to reach acceptable electric and electrochemical performance
- Assess the environmental performance of the short stack operated at different power outputs
- Compare the short stack performance with that of the commercial full scale micro-CHP system produced by the same manufacturer

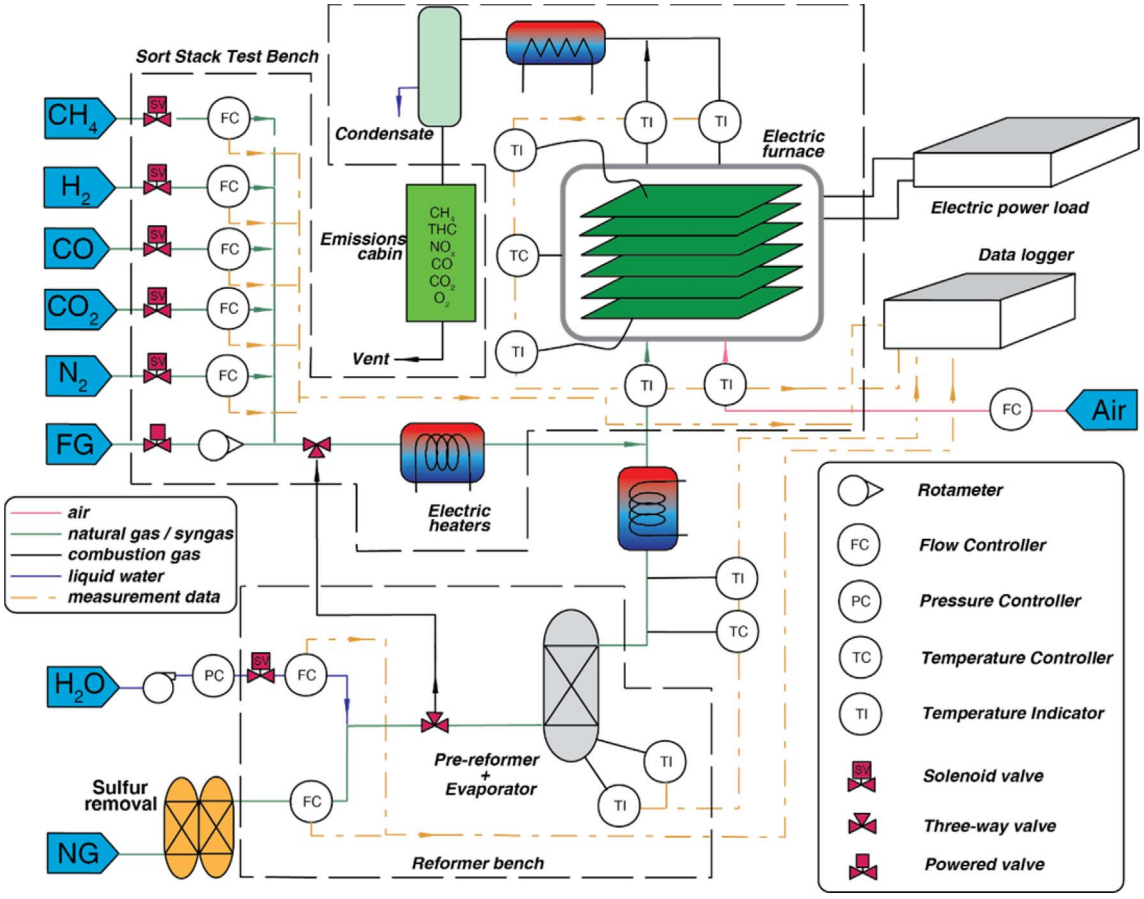

Fig. 1. Schematic of the test bench process flow, including the most important instrumentation probes.

2. Experimental

2.1. Set-up and instrumentation

The Short Stack Test Bench (SSTB) employed in the experimental analysis is manufactured by SOLIDpower S.p.a (Italy). It is made up of an electric furnace containing a 6-cell stack in a co-flow flow-field arrangement. The cells are made up of a thin 8 mol% Y_2O_3 stabilised Zirconia (YSZ) electrolyte (8 ± 2 μm) supported on a conventional porous Ni/YSZ anode electrode (240 ± 20 μm) [26]. The cathode electrode (40 ± 10 μm) is comprised of a composite of metallic perovskite Sr-doped $LaMnO_3$ (LSM) and oxide-ion electrolyte YSZ. The active area of each cell is 80 cm^2, equal to that of the cells employed in the micro-CHP systems of the manufacturer.

The stack can be fed either by the natural gas grid or by a mixture of technical gases, including H_2, CO, CO_2, N_2 and CH_4. The furnace is necessary to maintain the correct operating temperature of the stack, which could not be self-sustained otherwise. The temperature is controlled by an independent temperature controller (PIXSIS ATR621). The maximum allowed furnace temperature is set to 900 °C.

The stack is electrically connected to an electronic load (or a power supply for electrolysis operation) and a data logger. As far as the electric measurements are concerned, the system samples the value of each cell voltage and the overall current of the stack (sampling time period 10 s).

Each gas pipeline which supplies the technical gases is equipped with a valve and a Mass Flow Controller (MFC). The separate lines are then mixed together and humidified with steam (when it is supplied) before being fed to the anode inlet. The water line is supplied with deionised water and it is comprised of a ceramic filter, an emergency solenoid valve and an MFC. The natural gas line is made up of a low temperature desulphurisation unit (SulfaTrap™), an emergency solenoid valve and an MFC.

Upstream of the stack is a pre-reforming reactor that is fed by the water and natural gas lines, to ensure the partial conversion of CH_4 and larger hydrocarbons. Additionally, a gas pre-heater is employed in order to increase the anode inlet temperature to above 700 °C, when the pre-reforming reactor is operated at low temperature.

A schematic of the test bench process flow, including the most important instrumentation probes, is reported in Fig. 1. Moreover, a list of the instrumentation employed along with their uncertainty performance characteristics is reported in the Annex.

2.2. Operation

The SSTB can be operated in four different operating modes:

1. Operation with a mixture of technical gases and steam – SOFC mode
2. Operation with reformed natural gas and steam – SOFC mode
3. Operation with steam and technical gases for electrolysis – SOEC mode
4. Operation with carbon dioxide and steam for co-electrolysis – SOEC co-electrolysis mode

In the present study, only the second operating mode will be described and used, whilst operation with a mixture of technical gases will be covered in Part B of this work.

The most important constraints and flow requirements of the SSTB are reported in Table 1. These will have to be taken into account when designing the experimental procedures.

One of the effects of the constraints of Table 1 is relative to the procedure for garnering polarisation characteristic curves. In fact, at low current values, the need to maintain the fuel utilisation factor constant throughout the measurement of the polarisation curve, requires reducing the mass flow rates of the reactants; this is possible until the value of the flow meets the minimum value allowable by the MFC of each line. Consequently, the polarisation curves which will be shown in the following sections, will not show the voltage for very low current operation.

Table 1
SSTB constraints and flow requirements.

	Unit	Min	Max
Current	A	0	30
Temp	°C	–	800
S/C	–	2.0	–
U_f	%	–	85.0
NG	Nl/min	0.1	10
H_2O	g/h	20	200
H_2	Nl/min	0.1	10
N_2	Nl/min	0.1	10
CO	Nl/min	0.1	10
CO_2	Nl/min	0.1	10
Air	Nl/min	0.5	50

It should also be mentioned that the SSTB control system does not allow implementation of PID control changes on any of the operating variables. Therefore, the measured value is always affected by the ability of the on-board instrumentation to maintain the chosen set-point.

2.3. Methodology

2.3.1. Electrical and electrochemical performance optimisation

The cells which comprise the short stack are the same cells as those used in the 2.5 kW_e μ-CHP system called EnGEN™- 2500 as built by SOLIDpower S.p.a., whose performance characterisation has been discussed in previous work by some of the authors [1]. It is therefore interesting to study the short stack performance for operating conditions similar to those which characterise the nominal operation of the CHP system.

In order to do so, the steady state performance is explored by means of sensitivity analyses on the fuel utilisation factor (U_f) and the steam-to-carbon ratio (S/C). The former parameter is spanned from U_f = 65% to U_f = 85% at fixed S/C, whilst the latter from S/C = 2.0 to S/C = 3.0 at fixed U_f. For each operating condition the polarisation curve is produced. The furnace temperature has been fixed to 750 °C, which produces conditions that meet the requirements for maximum operating temperature of 800 °C.

2.3.2. Polarisation curve

The polarisation curve is one of the most important methods of assessing the performance of a fuel cell. Often it is also used as a validation foundation for detailed steady state cell and stack models which aim at spanning the entire current operating range. However, the exact procedure employed to measure such a curve is generally not discussed and its correct description is often lacking in the literature.

The procedure suggested by the manufacturer of the cells used in this analysis is characterised by a current step change of 1 A starting from the open circuit voltage (OCV or 0 A condition) and spanning the whole current range, up to 30 A. The fuel mass flow rate is calculated, according to the value of current, in order to maintain a constant fuel utilisation factor, U_f, as follows:

$$\dot{n}_{H_2,eq} = \frac{I * N_{cell}}{U_f 2F} \quad (1)$$

where, $\dot{n}_{H_2,eq}$ is the molar flow rate of equivalent hydrogen supplied to the whole stack and N is the number of cells in the stack. With the assumption that the composition of natural gas is 100% methane,[1] the molar flow rate of

[1] This assumption is limiting but it has been verified that the control system of the SSTB operates with it. In order to have a coherent response of the system to the supplied operating conditions, it has been chosen to maintain the same assumptions also in our calculations.

natural gas that should be supplied to the stack is:

$$\dot{n}_{NG} = \frac{\dot{n}_{H_2,eq}}{4x_{CH_4}} = \frac{\dot{n}_{H_2,eq}}{4} \tag{2}$$

As far as the air molar flow rate is concerned, it can be calculated once the oxidant utilisation factor of the stack is chosen. The desired oxidant utilisation is U_{ox} = 15.8% in order to reproduce the operating conditions of the CHP unit EnGEN™- 2500. Hence,

$$\dot{n}_{Air} = \frac{I}{4F}\frac{N_{cell}}{U_{ox}x_{O_2}} \tag{3}$$

Moreover, the steam mass flow rate is also changed in order to meet the requirements on the imposed S/C ratio.

$$\dot{n}_{H_2O} = \dot{n}_{NG} * S/C \tag{4}$$

An important parameter that is not usually mentioned in the standard procedure is the wait time between each current step change; in the reference methodology, the wait time is suggested to be of 1 min for sampling purposes.

In this study, attention is paid to the dynamic response of the short stack and system to each step change in current to ensure that the correct representation of the steady state behaviour of the cells is measured. It is found, in fact, even inside of a furnace for controlling temperature, that the short stack possesses a very significant thermal time constant for achieving steady state performance. Thus, the following modifications and changes to the suggested procedure are adopted and are recommended:

i) the air utilisation factor is kept constant, by changing the air mass flow rate according to the current value;
ii) the minimum wait time is not assumed a priori but it is determined in order to ensure steady-state conditions for the variable with the longest time constant[2]: in this case the measured parameter of interest that affected the measured performance with the longest time constant was the cathode outlet, which temperature should vary no more than ± 0.5 °C during the sampling time period;
iii) the sampling time starts only after the wait time is concluded and each wait time is determined in relation to the sampling rate in order to ensure a statistically relevant steady state sample;
iv) each current point is repeated multiple times (we selected at least three samples) in order to ensure the robustness of the measurement (see also the following section dedicated to post-processing procedures) and assurance of steady-state conditions.

It will be shown that, despite the experimental features of a temperature control system and electric furnace enclosure, these changes are necessary in order to guarantee a meaningful and repeatable measurement of the polarisation curve representing the steady-state operating conditions of the stack.

The described procedure would ensure that the polarisation behaviour described by the characteristic curves of the stack represent the real steady state performance, thus taking into account any stack dynamic responses that take considerable time associated especially with changes in local current production and temperature (typically the longest time constants), fluid flow dynamics (shorter time constants), and electrochemical dynamics (shortest time constants) [27].

2.4. Post-processing analysis

The measurements post-processing methodology has been developed in accordance with the standard procedure of the Laboratory of Micro-Cogeneration (LMC) at Politecnico di Milano [28]. The procedure is divided into two main steps: i) statistical analysis of the measurement data; ii) thermodynamic and electrochemical analysis.

Statistical analysis is of fundamental importance in experimental procedures. The measurement of a single act or phenomenon for specific operating conditions might not represent the average or typical behaviour of the system under those conditions; this is due to the presence of numerous uncontrollable effects that might bias the measurement. Only a randomised and repeated measurement may ensure an effective representation of the average behaviour of the system.

The first step in the statistical characterisation of each sample is the normality check according to the Normal population distribution. A Shapiro-Wilk test is usually performed for this purpose. However, it is often found that the normality hypothesis is not satisfied, mainly due to the limited size of the considered sample. On the other hand, when fitting the population distribution, a higher confidence interval is usually found with a t-Student distribution. Therefore, in this study all the confidence intervals at 95% will be expressed according to a t-Student distribution with 6 degrees of freedom.

$$\bar{x} - \frac{t_{95\%,6} * s}{\sqrt{N}} \le \mu \le \bar{x} + \frac{t_{95\%,6} * s}{\sqrt{N}} \tag{5}$$

The next step in the analysis of the single measurement sample is the check on the stationary requirements, as already mentioned above (in this case, the main focus is on the dynamics of the cathode outlet temperature). Once these checks have been completed the main statistical parameters of each sample can be calculated comprising of the mean, variance, minimum and maximum values, quantiles, percentage of outliers, mean without outliers, etc.

Prior to starting the thermodynamic and electrochemical analysis of the measurements, it is necessary to define and calculate the propagation of uncertainties for every measured variable. In this work, each value of direct absolute uncertainty is associated with the mean value for each variable in each sample, according to the instrumentation uncertainties list reported in the Annex. This procedure, despite not being rigorous from a theoretical point of view (since it associates the absolute uncertainty of the direct measure to a calculated value – the mean), is more conservative: the uncertainty of the mean value would be, in fact, lower than that of the direct measure.

The second step of the post-processing analysis is the thermodynamic and electrochemical elaboration of the measurements. The main performance parameters calculated in this step are: actual inlet fuel composition, Nernst potential, stack average voltage, current density, equivalent inlet hydrogen, S/C ratio, fuel and air utilisation factors and power output. Furthermore, the following efficiencies are also defined, respectively, first law efficiency η_I, ideal efficiency η_{id}, voltage efficiency η_V, and current efficiency η_C, as follows:

$$\eta_I = \frac{\dot{W}_{el}}{\dot{n}_{fuel} LHV} = \frac{VI * N_{cells}}{\dot{n}_{fuel} LHV} \tag{6}$$

$$\eta_{id} = \left|\frac{\Delta G_r}{\Delta H_r^{\circ}}\right| = \frac{E_N 2F}{LHV} \tag{7}$$

$$\eta_V = \frac{V}{E_N} \tag{8}$$

$$\eta_C = \frac{i}{i_{max}} \tag{9}$$

where, $i_{max} = \dot{n}_{H_2,eq} * 2F$ is the maximum current density obtainable if the total amount of equivalent hydrogen at the cell inlet was completely oxidised, N_{cells} is the number of cells which make up the stack and E_N is the Nernst potential, calculated as follows:

$$E_N = E_0(T_{ao}) + \frac{R * T_{ao}}{2F} \ln \frac{x_{H_2} x_{O_2}^{0.5}}{x_{H_2O}} \tag{10}$$

where T_{ao} is the temperature of the anode outlet. The ideal efficiency

[2] The time constant is defined as the minimum time to reach 99% of the stationary value for each variable.

examines the difference between the ideal electrochemical work produced by the cell and the chemical energy of the fuel available at its inlet, which is assumed to equal the fuel mass flow times the Lower Heating Value (LHV). Despite the differences in various definitions, it must be always verified that the ideal efficiency is greater than the first law efficiency; this is due to two main effects, considered in the definitions of the voltage and current efficiencies: the presence of the cell irreversibilities, which lower the ideal potential to obtain the useful cell voltage, and the effect of the fuel utilisation factor, which entails that the supplied fuel is not entirely oxidised.

The current efficiency coincides with the fuel utilisation factor.

For all the mentioned calculated variables the propagation of errors is calculated using the conventional rules of propagation of uncertainty [29].

As already mentioned, each operating condition has been tested at least three times in order to have a reasonable redundancy of the measured data. This procedure ensures a higher robustness of the population and more independence to external concurrent and uncontrolled phenomena. Therefore, the final step of the procedure is the compatibility check on the main performance parameters.

The compatibility check is very important to determine whether some of the tests considered shall be considered valid or should be discarded as outliers. The procedure compares each variable characterised by its expanded uncertainty with the 95% confidence interval calculated on the population distribution. If the variable is not consistent with the average behaviour of the system, the compatibility check shows a warning, which may suggest that the specific measurement should be excluded from the analysis. An example of a successful compatibility check is shown in Fig. 2.

3. Results and discussion

In this section the procedure to perform a polarisation curve on a short stack is revised compared to the reference and most commonly used procedure. Since the minimum sampling time allowed by the control interface is 10 s, the standard overall sampling time of 1 min does not allow sufficient time reach steady state and achieve a statistically representative number of measurements. Therefore, in this work the sampling time is increased in order to garner a size of the sample of at least 100 measurements. Moreover, the need to represent real stationary operation of the stack, per each current point, requires an increase in the time between two current step changes. Otherwise, there would be the risk to report polarisation curves in which the cells are in a transient operation condition governed by dynamics (due to issues of stabilisation of thermal, local current, and composition profiles) which may bias the measurement.

In this study, an additional wait time between the current step change and the sampling time is therefore included; this time range allows the stack to stabilise and reach a stationary condition. The wait time should be changed depending upon the magnitude of the current step change.

Fig. 3 shows three polarisation curves obtained for the same operating conditions but with different wait times between each current step change. The sampling time is fixed at 20 min for the 15 min and 45 min wait time cases and to 5 min for the 5 min wait time case. The reason for this difference in sampling time is that the stack dynamics are largest during the first 20 min subsequent to the current step change; therefore, had the sampling time been kept at 20 min even for the shortest wait time, the difference in the voltage sample would have been averaged out and the real voltage measurement after the current step change would have been lost.

With a small wait time (5 min), the stack does not have the time to reach a steady-state condition from a thermal balance perspective; this affects the local temperature and composition, thus the Nernst potential and hence the voltage measurement, entailing its non-negligible overestimation. It is also shown that the cases with 15 min and 45 min of wait time are not characterised by major differences in the voltage measurement. This helped in setting the value of minimum wait time for a current step change of 1 A–15 min.

3.1. Short stack temperature dynamics

In order to assess the effect of the operating temperature on the voltage measurements during variable current operation, a specific set of tests is conducted. The behaviour depicted in Fig. 3 suggests the presence of a measurement hysteresis effect on the voltage measurements due to temperature variations (since it was observed that the only measured variable that took so long to stabilise was the cathode exit temperature). Therefore, tests are carried out using the same testing procedure for polarisation curves suggested by the manufacturer (as reported above), which minimises the wait time between each current step change (1 min). Hysteresis curves are produced for each of the main operating conditions (different U_f and S/C). The upward polarisation curve branch shows the behaviour of the cells when the current is increased by 1 A for each step change, whilst the downward branch, which measurements were made immediately after the first set, is produced by a reduction of 1 A for each step change. In this way, a voltage-current curve is produced in each direction starting and ending

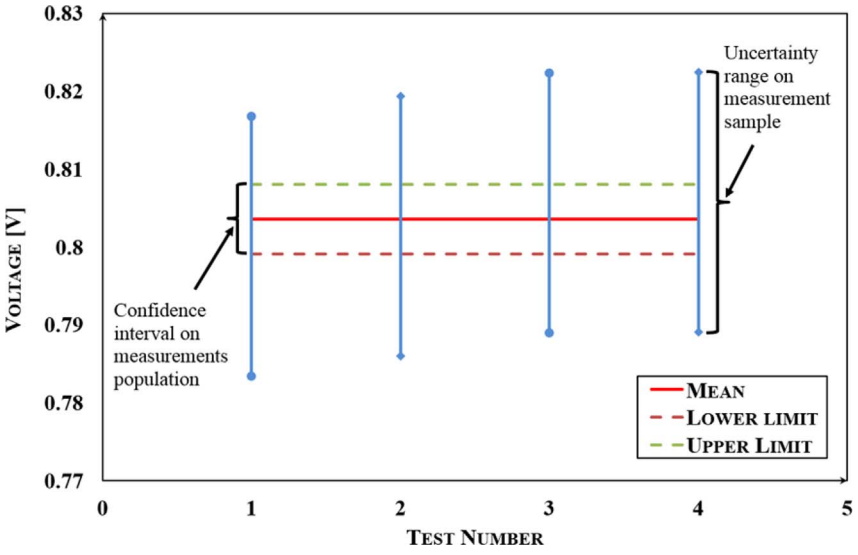

Fig. 2. Example of compatibility test on the average stack voltage.

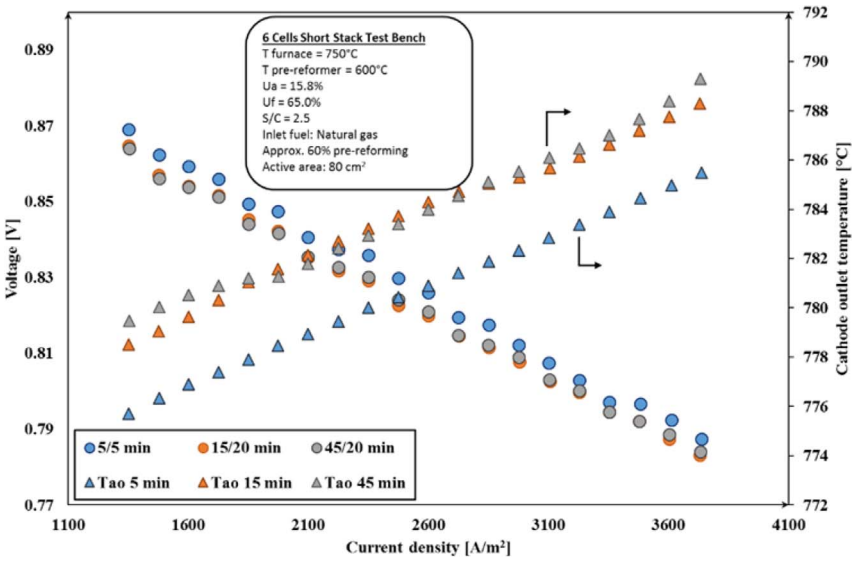

Fig. 3. Three polarisation curves obtained for the same operating conditions but with different wait times between each current step change.

at the OCV condition.

One of the resulting hysteresis curves for the case at $U_f = 65\%$ and $S/C = 2.0$ is reported in Fig. 4. Each dot represents the average measurement during the 1 min sampling time. The voltage is the average of the voltage measurements of the six cells. As far as the post-processing analysis is concerned, the figure reports the semi-band of the absolute uncertainties for each direct measure, using the data reported in the Annex.

It is clear from the curves reported in Fig. 4, that the measured voltage dependence upon current is influenced by a change in the cell operating temperature (here represented by the cathode outlet stream temperature). As the current increases for the upwards V-I curve the operating temperature (red diamonds) is steadily increasing as a result of insufficient time to achieve thermal steady-state of the cells. The short stack thermal response, even inside of a furnace, is not fast enough for the temperature to level off to a stable value after each current step change. It is clear that the steady state temperature and measured voltage for each value of current would be higher compared to the measured one as current is increased, had enough time been given to the cell to reach a stable condition. Subsequently, the downwards polarisation curve is acquired by progressively reducing current. In this case, the cell starts at 30 A/3750 A/m^2 with a thermal inertia which makes the temperature rise even as the current is being reduced. Only when the current is below 20.8 A/2600 A/m^2 does the temperature start to decrease due to the reduction of the current allowing the related lower heat generation to overcome the thermal inertia of the stack.

The net effect of this heat generation, thermal inertia balancing phenomenon is that the two polarisation curves are acquired at different temperature distributions at each current level; none of which are equivalent to the steady-state temperature of the short stack. Thus, neither curve represents steady state performance, which affects the evaluation of the Nernst potential and all electrochemical losses that contribute to the voltage measurement. It is observed for every operating condition tested that the downward polarisation curve always underestimates the voltage compared to upward one, despite the temperature is higher. This behaviour is not expected since the higher temperature (although the variations are limited to less than 10 °C) should lead to a reduced ASR, allowing a certain increase of voltage for the same current density and reactant flow rates. However, this expected theoretical behaviour is confounded by several factors: (i) the recording of values reflects a dynamic condition, where the frequency response of the specific test stand, the measurement probes and other dynamic phenomena should be taken into account; (ii) during the tests the furnace temperature setting is kept constant, while the temperature signal considered to estimate the achievement of steady-state conditions is referred to the cathode gas outlet. Therefore, it is likely that the stack operates with a non-uniform temperature field which also complicates the observed phenomena; (iii) a capacitance effect, mainly related to water mass transport in the thick anode, may appear in the voltage response to the current step change. As an example, some references [30,31] report an increased anode impedance due to limited H_2O counter-diffusion in the anode porous structure, so that at increasing current density the augmentation of the produced H_2O in the anode reaction site may yield higher polarisation losses, contributing to hinder the temperature effect.

The main conclusion which can be drawn from this analysis is that, despite the stack temperature being primarily controlled by a furnace, the temperature dynamics of a short stack in response to even small changes in current are on the order of many minutes to hours. Therefore, even in a controlled furnace environment, these thermal dynamics cannot be neglected for a correct and precise measurement of the steady state polarisation behaviour. In order to address this, the polarisation curves described in the next sections have been carried out using the procedure described in the methodology section, keeping the

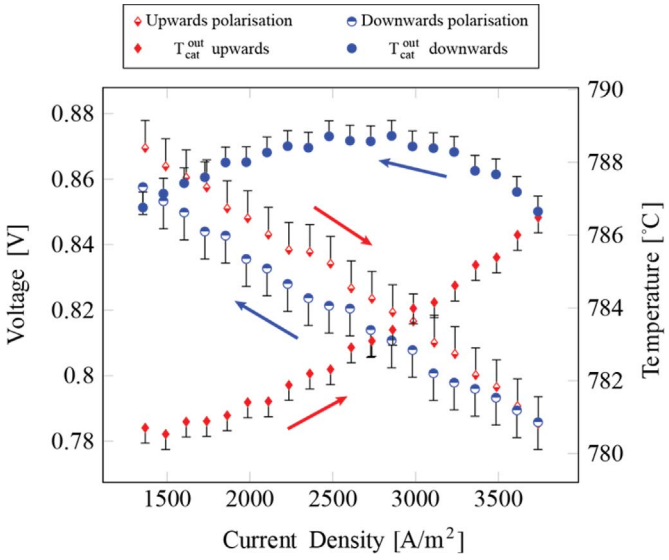

Fig. 4. Two consecutive and inverse polarisation curves showing a hysteresis behaviour due to the effect of the temperature on the voltage (measured temperature at air stream outlet, T_{ao}).

sampling time and wait time long enough to assure statistically valid measurements that minimise the effects of stack temperature dynamics on the voltage measurements.

It is worth noting that an effect of stack temperature variation vs. current was also observed by *Yu* et al., 2017 [32] although the reported behaviour was different (decrease of temperature with current), possibly due to differences in the test procedures and in the control of the air flow rate. The existence of such changes, however, indirectly confirms the opportunity of adopting special care in the identification of steady state conditions during the V-I measurements.

3.2. Electrochemical performance characterisation

Fig. 5 reports the average V-I curves and the corresponding power density curves at different S/C and U_f. In particular, each subfigure reports the stack performance at different S/C for a constant value of U_f. The error bars reported in the picture represent the confidence interval at 95% for each plotted variable, calculated as previously explained. As reported in the "Operation" section of the paper, the polarisation curves reported in Fig. 5 are characterised by a minimum current density higher than 0 A; the minimum value of current density which is possible to test depends on constraints imposed by the MFCs reported in Table 1. In fact, in order to maintain a constant fuel utilisation factor throughout the curve it is necessary to change the mass flow rates which eventually hit the constraints of the MFCs when the current densities get low enough.

As far as the reported Nernst potential is concerned, its calculation according to Eq. (10) may be practically ambiguous due to the fact that the fuel composition at the stack inlet is not measured in the experimental setup. In order to calculate the ideal potential, a 0D equilibrium model comprising the pre-reformer and the cell is employed. At OCV, the stack current is nought and therefore the conversion of the fuel constituents is also zero. Consequently, the limiting Nernst potential in this condition is assumed to be dependent on the inlet H_2 molar fraction. On the other hand, when the stack operates at any other point on the polarisation curve, the conversion of the fuel species would entail a leaner fuel mixture at the stack outlet, as far as the H_2 concentration is concerned. Therefore, with the assumption of equipotential electrodes, the most limiting Nernst potential occurs at the stack outlet, for a co-flow streams layout.

The model is employed to calculate the fuel stream composition for each point on the polarisation curve and the outlet H_2 molar fraction is used to calculate the Nernst potential.

Notice that the calculation of the stack inlet composition and the Nernst potential associated to it, must be respectful of the measured OCV for each operating condition. It is verified that the composition resulting from an equilibrium calculation of the pre-reforming reactor at 600 °C, would not meet this requirement. The possible reasons for the

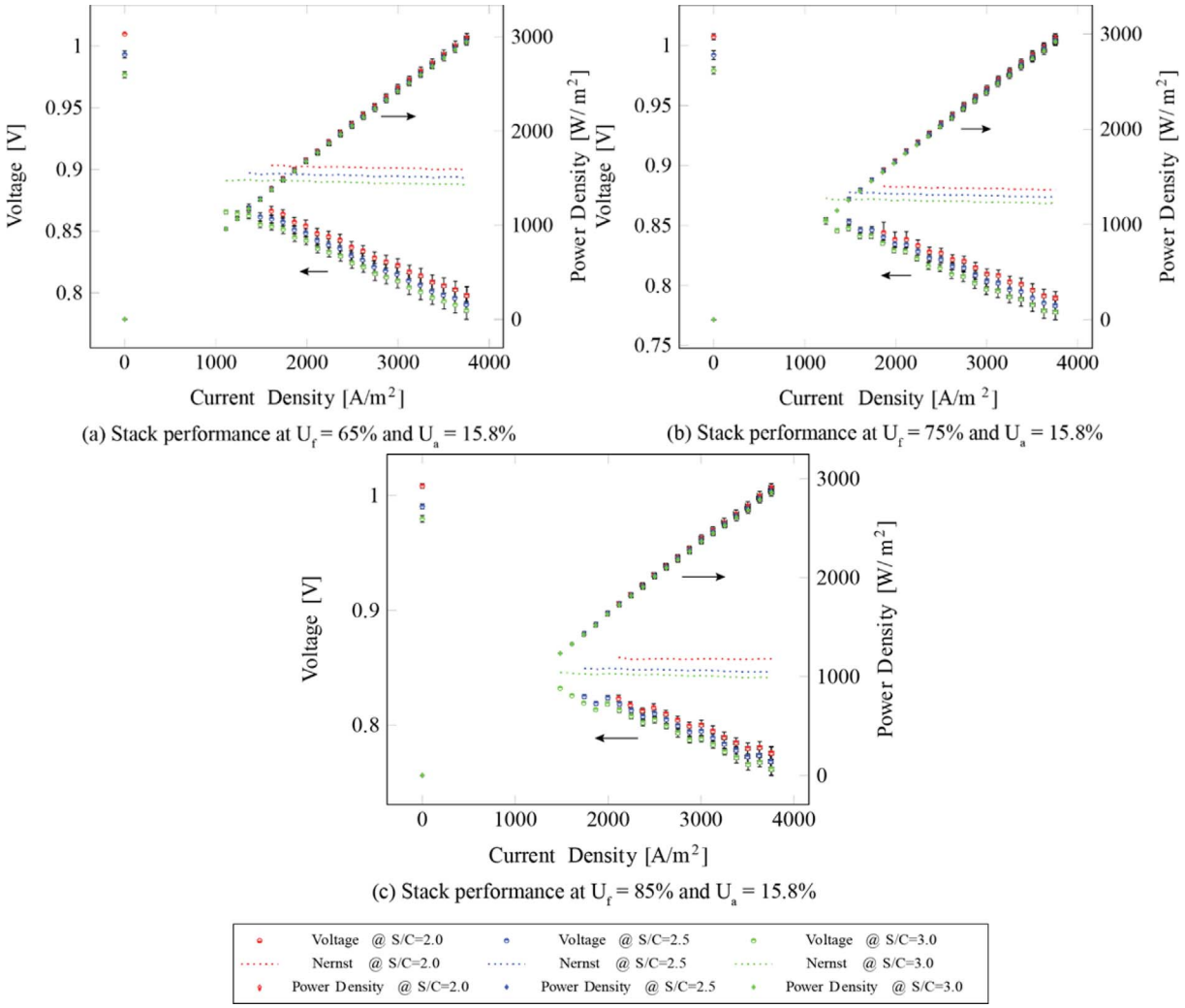

Fig. 5. Polarisation curves and power density profiles from the sensitivity analysis on the stack S/C and U_f. Furnace temperature = 750 °C; Pre-reformer temperature = 600 °C. Note that Figure 5c, shows voltage steps in the polarisation curve which are related to the inherent control of mass flow controllers; this effect is more visible in these operating conditions because of the lower mass flow rates which characterise the case at U_f = 85%.

discrepancy with the experimental settings may be related to the fact the section of the test stand between the pre-reformer exit and the stack inlet allows increasing the temperature of the fuel stream up to the measured anode inlet temperature which, for all the spanned operating conditions, is above 770 °C.

Following this methodology, it is verified that the pre-reforming equilibrium temperature which allows meeting the measured OCV value for each operating condition is 700 °C.

This simplified approach allows calculating a reference value of voltage to which compare the actual performance of the stack for each operating condition.

From the analysis of the polarisation curves, it is clear how the measured voltage decreases for a fixed value of current density as S/C ratio is increased. Considering the example of U_f = 65% at I = 24 A, the relative voltage reduction between the case at S/C = 2.0 and that at S/C = 3.0 is 1.54%. The reason is almost fully explainable by a reduction of the Nernst potential, which reduces by 1.36%. This suggests that the OCV reduces more than the Nernst potential with increasing steam concentration in the inlet fuel. Consequently, the overall net effect is a reduction in the voltage performance. This is also evidenced in the electric efficiency variation which reduces by about 1.61% from S/C = 2.0 to 3.0, as shown in Fig. 6.

As far as the sensitivity analysis on the fuel utilisation factor is concerned, the results show a higher voltage performance at lower U_f, which can also be confirmed by the higher voltage efficiency reported in the Fig. 6b. However, the much more dominant rise of the current efficiency at higher U_f indicates that the overall electric efficiency increases with increasing U_f. This trend is expected due to the higher amount of equivalent hydrogen that is electrochemically converted in the anode channel when the utilisation factor is increased. On the other hand, the open circuit leakage losses remain unchanged at different U_f, since both the OCV and Nernst potential are not affected by the value of fuel utilisation factor.

Fig. 6c reports the comparison of the stack electric efficiency measured in this study with those reported by *Wuillemin* et al. *2014* [33] for their SOLIDpower S.p.a. 50-cell stack fed with pre-reformed natural gas at different utilisation factors. The two curves show a close match between the two stacks confirming that the use of short-stacks embodies a very good representation of the expected performance of full scale stacks. The slight differences in the efficiency values noticeable in Fig. 6

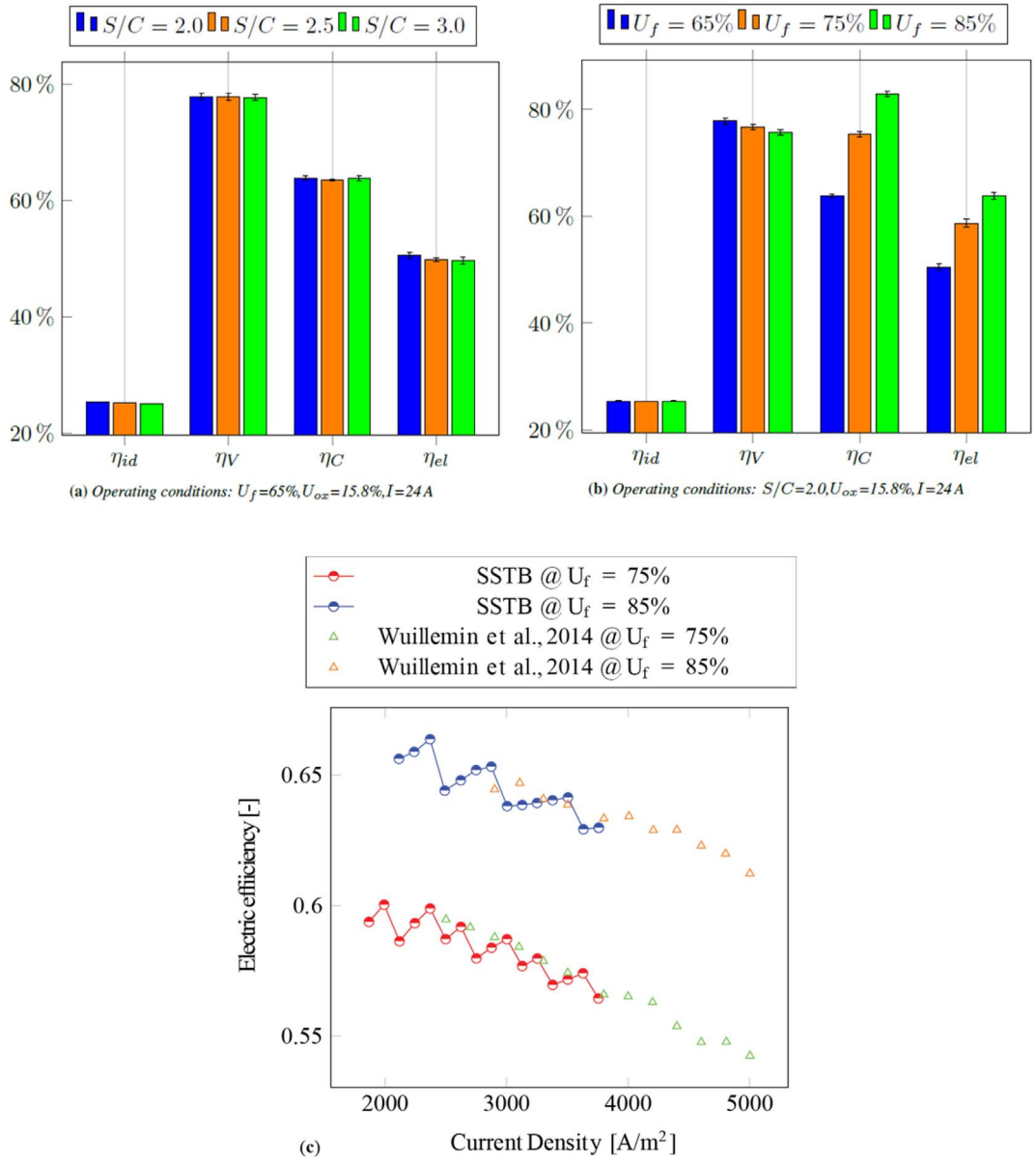

Fig. 6. Efficiencies profiles at different S/C (a) and U_f (b). (c) Electric efficiency comparison with literature data from Wuillemin et al., 2014 [33].

Table 2
Summary of the most important input and output operating parameters at 24 A (3000 A = m2) for every U_f and S/C.

		Current density	Voltage	E Nernst	SC	U_f	U_a	Power	Air	H_2O	CH_4
		[A/m^2]	[mV]	[mV]	[−]	[%]	[%]	[W]	[ml/min]	[g/h]	[ml/min]
						U_f = 0.65					
S/C	**2**	2995.57 ± 21.51	822.40 ± 5.35	901.4ǂ	1.98 ± 0.01	63.84 ± 0.34	15.79 ± 0.11	118.25 ± 1.59	15109.41 ± 7.64	37.43 ± 0.07	392.40 ± 1.05
	2.5	2986.08 ± 6.33	815.16 ± 5.58	894.7ǂ	2.47 ± 0.01	63.51 ± 0.12	15.74 ± 0.03	116.84 ± 0.76	15107.02 ± 9.13	46.87 ± 0.06	393.23 ± 0.78
	3	2995.46 ± 19.57	809.76 ± 5.53	889.1ǂ	2.97 ± 0.01	63.80 ± 0.42	15.79 ± 0.09	116.43 ± 1.48	15104.96 ± 11.56	56.18 ± 0.06	392.68 ± 0.98
						U_f = 0.75					
S/C	**2**	3001.75 ± 22.98	809.64 ± 4.19	880.5ǂ	2.03 ± 0.00	75.38 ± 0.50	15.83 ± 0.12	116.66 ± 1.45	15106.36 ± 2.65	32.58 ± 0.07	333.02 ± 0.64
	2.5	3000.13 ± 19.09	803.54 ± 4.44	874.6ǂ	2.52 ± 0.01	75.34 ± 0.52	15.82 ± 0.10	115.72 ± 1.36	15105.25 ± 5.2	40.50 ± 0.12	333.01 ± 0.32
	3	2994.60 ± 23.74	796.94 ± 4.5	869.2ǂ	3.04 ± 0.01	75.15 ± 0.59	15.79 ± 0.12	114.55 ± 1.45	15102.87 ± 2.3	48.80 ± 0.09	333.26 ± 0.07
						U_f = 0.85					
S/C	**2**	3003.80 ± 24.22	800.15 ± 4.22	857.9ǂ	1.98 ± 0.01	82.89 ± 0.56	15.84 ± 0.14	115.37 ± 1.38	15105.30 ± 12.6	28.87 ± 0.07	303.04 ± 0.78
	2.5	3003.09 ± 21.32	794.83 ± 4.12	847.9ǂ	2.45 ± 0.00	82.95 ± 0.55	15.83 ± 0.10	114.57 ± 1.36	15105.61 ± 9.36	35.80 ± 0.06	302.79 ± 0.30
	3	3003.80 ± 22.13	788.31 ± 2.86	843.2ǂ	2.94 ± 0.01	82.94 ± 0.57	15.84 ± 0.12	113.66 ± 1.23	15107.56 ± 3.84	43.00 ± 0.10	302.87 ± 0.35
		Furnace	Reformate	Evaporator	Reformer	T_{ai}	T_{fi}	T_{ao}	T_{fo}	TT	TB
		[°C]	[°C]	[°C]	[°C]	[°C]	[°C]	[°C]	[°C]	[°C]	[°C]
						U_f = 0.65					
S/C	**2**	749.57 ± 0.07	192.73 ± 0.74	270.70 ± 0.01	600 ± 0	773.41 ± 2.58	768.38 ± 2.7	790.49 ± 2.95	776.48 ± 2.73	787.52 ± 3.35	774.14 ± 2.55
	2.5	749.53 ± 0.05	192.1 ± 0.21	271.39 ± 0.03	600 ± 0	774.56 ± 2.7	768.90 ± 2.85	791.45 ± 3.16	777.60 ± 2.9	788.21 ± 3.68	774.82 ± 2.81
	3	750.16 ± 2.13	192.3 ± 1.09	273.12 ± 0.06	600 ± 0	774.85 ± 2.76	768.49 ± 2.91	791.76 ± 3.19	777.96 ± 2.91	788.38 ± 3.79	774.86 ± 2.88
						U_f = 0.75					
S/C	**2**	749.54 ± 0.04	193.31 ± 0.22	270.6 ± 0.05	600 ± 0	774.50 ± 2.80	769.27 ± 2.56	790.97 ± 3.19	776.91 ± 2.9	787.84 ± 3.87	774.44 ± 2.87
	2.5	749.52 ± 0.06	193.1 ± 0.79	270.8 ± 0.11	600 ± 0	775.20 ± 2.84	769.56 ± 2.8	791.7 ± 3.07	777.66 ± 2.9	788.47 ± 3.5	774.85 ± 2.85
	3	749.57 ± 0.04	192.33 ± 0.79	271.57 ± 0.06	600 ± 0	775.58 ± 2.50	769.41 ± 2.5	791.95 ± 2.77	778.06 ± 2.59	788.45 ± 3.04	774.88 ± 2.52
						U_f = 0.85					
S/C	**2**	749.55 ± 0.05	192.79 ± 0.76	270.54 ± 0.04	600 ± 0	775.41 ± 3.32	770.17 ± 3.26	791.51 ± 3.66	777.42 ± 3.46	788.27 ± 4.07	774.86 ± 3.31
	2.5	749.55 ± 0.04	192.74 ± 0.37	270.68 ± 0.04	600 ± 0	776.15 ± 3.15	770.48 ± 3.13	792.19 ± 3.40	778.17 ± 3.2	788.91 ± 3.93	775.36 ± 3.15
	3	749.51 ± 0.03	192.94 ± 0.39	271.00 ± 0.08	600 ± 0	776.29 ± 3.26	770.21 ± 3.2	792.28 ± 3.46	778.35 ± 3.3	788.87 ± 3.84	775.26 ± 3.16

ǂ Simulated values - uncertainty not available.

are, in fact, only related to the control logic of the reactants mass flow rates of the SSTB.

As far as the stack performance at low current densities is concerned, the correct evaluation of the activation losses contribution would require the use of a cell model or an impedance spectroscopy test. Finally, it should be noticed that no concentration overpotential losses region is observed at the highest current values.

Finally, in Table 2 a summary of the most important input and output operating parameters are reported with reference to the case at 24 A (3000 A/m^2) for all U_f and S/C values explored in the analysis.

3.3. Comparison with CHP system

Finally, a comparison between the polarisation performance of the short stack and the μ-CHP plant EnGEN™- 2500 (see Ref. [28]) is reported in Fig. 7. It should be remembered that the two systems are characterised by the same type of cells, having an active area of 80 cm^2.

The polarisation curve of the CHP plant (tested at the National Fuel Cell Research Center) is obtained for six current points ranging from the OCV to 26 A. The operating conditions are similar to those used in the SSTB; in particular, the stack is supplied with natural gas that is pre-reformed at 600 °C. The utilisation factor has been fixed to 75.0%. It should be noted that these measurements were acquired for a small difference in the S/C ratio between the SSTB and EnGEN™- 2500; however, due to the aforementioned considerations, the effect of this difference is not expected to significantly impact the voltage profile. A greater effect could be expected on the efficiency values which would be slightly underestimated compared to a case at higher S/C.

From Fig. 7, the same trend in the voltage performance for the two systems is noticeable. A small difference is detected between the average voltage of the left and right hand side stacks of the CHP system. However, the slightly higher value of the right hand side stack is a usual behaviour already measured during the experimental campaign reported in *Mastropasqua* et al. *2016* [28]. The two systems are characterised by the same cells; however, differences between a full-scale stack and a short-stack may comprise of the following:

- Different vertical thermal gradients along the height of the stack, due to the different number of cells per stack of the full-scale with respect to the short-stack
- Heat losses effects: (i) the full-scale system features a different area/volume ratio with respect to the short stack, and (ii) the short stack is operated in a heated furnace
- Probable effect of non-uniform flow distributions from the stack manifolds
- Differences in the inlet reactant flow temperatures which are not directly controllable on the SSTB
- Small differences amongst cells and between cells as installed against an end-plate versus the middle of the stack

All things considered, the two measurements show remarkably similar performance between the SSTB and EnGEN™- 2500 stack measurements, signalling a negligible effect of the reported points on the two stacks overall performance.

As far as the electric efficiency comparison is concerned, the same trend at increasing current density is obtained for the short stack and the average efficiency of the two stacks, which the CHP system is comprised of. The slightly lower efficiency of the CHP system reflects the already mentioned difference in the voltage performance.

In order to complete the comparison, Fig. 8 reports the result of a single measurement test for the environmental performance analysis during the measurement of a polarisation curve on the SSTB. The reader should remember that the emission measurements have been collected downstream the mixing and cooling of the anodic and cathodic stream of the short-stack, as represented in Fig. 1. In the same figure, the exhaust composition of the CHP system has been plotted during its nominal operation as measured in Ref. [28].

The difference in NO emissions between the short stack and the CHP system is primarily noticeable from Fig. 8a, which differ by a full order of magnitude. The CHP system NO emission is approximately equal to 5 ppm at nominal operation, whilst the short stack ranges between 5 and 8 ppb across the entire polarisation curve. This significant difference is due to the presence of a burner in the CHP system that is continuously supplied with supplemental natural gas to completing the oxidation of the anodic off-gas. Such an anode off-gas burner with supplemental firing (whose thermal input can be partly recovered for cogeneration) is not present in the SSTB. Therefore, it shall be clearly understood that pure SOFC systems, including those that have anode off-gas oxidizers without supplemental fuel provided, are able to reach extremely low values of NO emissions (on the order of less than 10 ppb).

On the other hand, the value of CO emissions from the short-stack are of the order of 0.5–1 v/v% across the polarisation curve, as reported in Fig. 8b. The CHP CO emissions have been measured at 14.4 ± 4.8 ppm under nominal operating conditions. This limited value is related to the presence of the anodic off-gas burner - not present in the short-stack test stand – which allows completing the oxidation of most of unburned fuel in the anode stream.

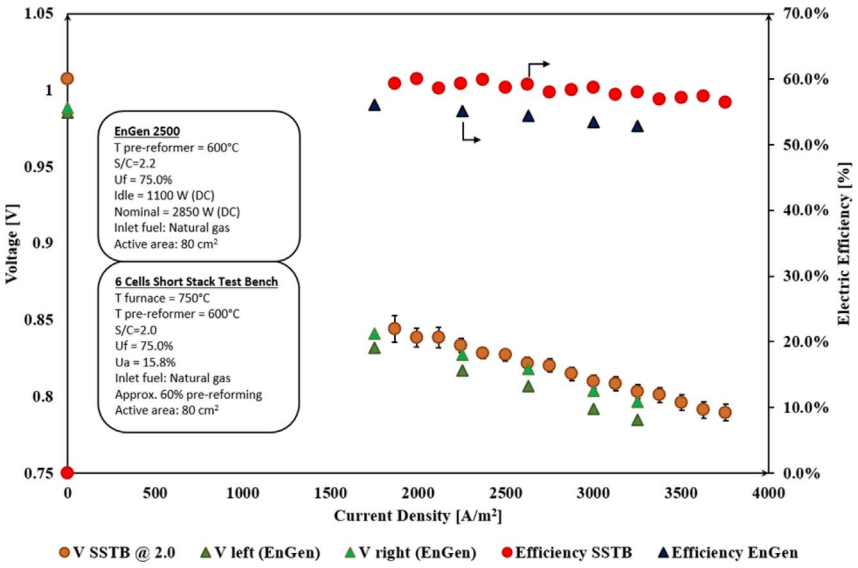

Fig. 7. Comparison of the polarisation performance and electric efficiency of the SSTB with the μ-CHP system EnGEN™- 2500.

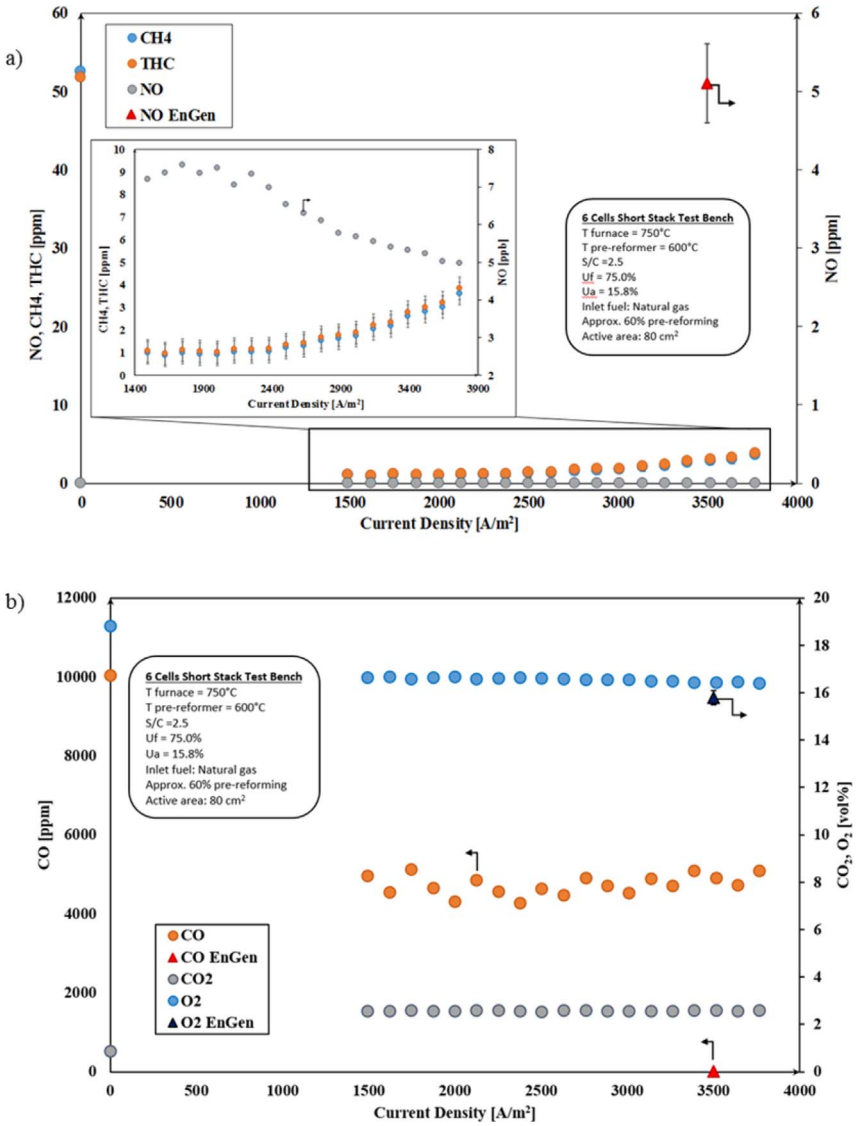

Fig. 8. Emissions of CH_4, THC, NO (a) and CO, CO_2 and O_2 (b) from the SSTB and from the μ-CHP system EnGEN™- 2500.

Finally, the similar value of O_2 molar fraction in the exhaust gases measured for both systems confirms that the air utilisation factor has been maintained constant and equal to that of the CHP system for all of the reported tests. The EnGEN™- 2500 exhibits slightly lower O_2 molar fraction due to the supplemental firing.

4. Summary and conclusions

The present work completes an experimental characterisation of an SOFC short-stack and the analysis of its performance operating conditions of interest for commercial SOFC systems. The work is carried out at the National Fuel Cell Research Center (NFCRC) at the University of California, Irvine employing the Short Stack Test Bench (SSTB) manufactured by SOLIDPower S.p.a. (Italy). The study can be summarised in three sections: i) development of a complete measuring and post-processing methodology able to accurately represent the steady-state behaviour of the short-stack; ii) electrical and electrochemical characterisation of the short-stack employing a set of sensitivity analyses on S/C and U_f across the whole polarisation range; iii) thermodynamic and environmental comparison with a commercial micro-CHP unit. The main findings are:

- A new methodology is proposed to measure the polarisation performance of the short-stack which allowed the identification of the order of magnitude of the stack dynamic response to a current step change. This has also been verified by the hysteresis measured during acquisition of two consecutive and inverse polarisation curves; the hysteresis shape is due to the stack temperature effect on the voltage measurement.

In order to ensure a correct voltage measurement a wait time of at least 15 min is to be maintained for each current step of 1 A before starting the actual sampling. It is suggested that this wait time should be increased if the stack is made up of a larger number of cells.

- The sensitivity analysis on the S/C ratio and U_f have shown a measured voltage decrease for a fixed value of current density at increasing S/C ratios and a higher voltage performance at lower U_f. The former is almost fully explainable by a reduction of the Nernst potential; the latter is due to the higher amount of equivalent hydrogen which is available in the anode channel when the utilisation factor is decreased.
- The overall polarisation performance is comparable to that of the full stack employed in the μ-CHP system by the same manufacturer, confirming the good representation that short-stack analyses can give of the entire SOFC module.

The environmental performance is also measured verifying the

negligible values of NO emissions (< 10 ppb) across the whole polarisation curve. This result confirms that the NO emission levels measured in the EnGEN™- 2500 μ-CHP (≈ 5*ppm*) and reported in *Mastropasqua* et al., 2016 [28] are solely attributable to the anode off-gas burner present in the system and not to the SOFC stack.

Acknowledgements

The authors would like to thank the National Fuel Cell Research Center (NFCRC) for providing the experimental equipment and especially Dr. Li Zhao, Derek McVay and Rich Hack for their support and advice. The authors also deeply thank SOLIDPower S.p.a. and especially Dr. Francesco Ghigliazza for the support on the SSTB. Moreover, the authors would like to thank Naoki Nagura from Horiba Ltd. for his help in acquiring the exhaust gas emissions measurements. Finally, the authors thank Edison S.p.a for partly supporting the work related to this study within Politecnico di Milano Ph.D. program.

Annex

Property and Location	Manufacturer	Model	Uncertainty
Temperature		type K	± (0.03 + 0.05/100*|T|)
Reformate			
Furnace		type K	± (0.03 + 0.05/100*|T|)
Evaporator		type K	± (0.03 + 0.05/100*|T|)
Reformer		type K	± (0.03 + 0.05/100*|T|)
Air (inlet)		type K	± (0.03 + 0.05/100*|T|)
Air (outlet)		type K	± (0.03 + 0.05/100*|T|)
Fuel (inlet)		type K	± (0.03 + 0.05/100*|T|)
Fuel (outlet)		type K	± (0.03 + 0.05/100*|T|)
Top stack		type K	± (0.03 + 0.05/100*|T|)
Bottom stack		type K	± (0.03 + 0.05/100*|T|)
Mass Flow Rate	Vögtlin	Red-y Smart Controller GSC	± (0.5% RV)
Hydrogen			
Nitrogen	Vögtlin	Red-y Smart Controller GSC	± (0.5% RV)
Carbon Monoxide	Vögtlin	Red-y Smart Controller GSC	± (0.5% RV)
Carbon Dioxide	Vögtlin	Red-y Smart Controller GSC	± (0.5% RV)
Steam	Bronkhorst	IN-FLOW 112-Al	± (0.5% RV + 0.1% FS)
Natural Gas	Bronkhorst	IN-FLOW 112-Al	± (0.5% RV + 0.1% FS)
Air	Vögtlin	Red-y Smart Controller GSC	± (0.5% RV)
Emissions	Horiba	Portable Gas Analyzer PG-350E	± (0.5% FS)
		Ambient NOx monitor APNA-360	± (1% FS)
		Ambient HC monitor APHA-360	± (1% FS)
Electronic Load	Agilent	N3300A and N3306A	± (0.05% RV + 0.010)
Current			
Voltage			± (0.05% RV + 0.003)

References

[1] International Energy Agency (IEA), Energy, Climate Change & Environment - 2016 Insights, 9 rue de la Fédération 75739, Paris Cedex 15, France, 2016.
[2] International Energy Agency (IEA), World Energy Outlook 2016-Special Report: Energy and Air Pollution, (2016), http://dx.doi.org/10.1016/0013-9327(70)90009-1.
[3] I. Septemb, U.M. Hev, European fuel cell micro-CHP project milestone, Fuel Cells Bull. 2015 (2015) 1, http://dx.doi.org/10.1016/S1464-2859(15)30238-8.
[4] Ceres Power to trial SOFC home power in UK as part of ene.field, Fuel Cells Bull. 2016 (2016) 6, http://dx.doi.org/10.1016/S1464-2859(16)30274-7.
[5] New FCH JU project PACE will deploy 2650 micro CHP units, Fuel Cells Bull. 2016 (2016) 5, http://dx.doi.org/10.1016/S1464-2859(16)30140-7.
[6] D. Papurello, A. Lanzini, L. Tognana, S. Silvestri, M. Santarelli, Waste to energy : exploitation of biogas from organic waste in a 500 W el solid oxide fuel cell (SOFC) stack, Energy 85 (2015) 1–14, http://dx.doi.org/10.1016/j.energy.2015.03.093.
[7] A. Lanzini, H. Madi, V. Chiodo, D. Papurello, S. Maisano, M. Santarelli, et al., Dealing with fuel contaminants in biogas-fed solid oxide fuel cell (SOFC) and molten carbonate fuel cell (MCFC) plants: degradation of catalytic and electrocatalytic active surfaces and related gas purification methods, Prog. Energy Combust. Sci. 61 (2017) 150–188, http://dx.doi.org/10.1016/j.pecs.2017.04.002.
[8] Japanese group unveils SOFC Ene-Farm residential cogen unit, Fuel Cells Bull. 2012 (2012) 4, http://dx.doi.org/10.1016/S1464-2859(12)70093-7.
[9] NETL - DOE clean coal Research program, Solid Oxide Fuel Cells - Technol. Program Plan. (2013).
[10] Department of Energy, The Department of Energy Hydrogen and Fuel Cells Program Plan, 2011..
[11] B.M. White, W.L. Lundberg, J.F. Pierre, Accomplishments, status, and roadmap for the U.S. Department of Energy's Fossil Energy SOFC program, ECS Trans. 68 (2015) 23–38, http://dx.doi.org/10.1149/06801.0023ecst.
[12] Fuel Cell Energy, (n.d.). http://www.fuelcellenergy.com/.
[13] P. Margalef, Fuel cell technologies for power generation and energy storage, Next-generation Energy Storage Conf, 2017 San Francisco, California.
[14] Bloom Energy, Bloom Energy, (n.d.). http://www.bloomenergy.com/fuel-cell/solid-oxide/.
[15] Solid Power, (n.d.). http://www.solidpower.com/en/home/.
[16] Elcogen, (n.d.). http://elcogen.ee/new/en/.
[17] Ceres Power, (n.d.). http://www.cerespower.com/(accessed 11 21, 2016)..
[18] K. Föger, T. Rowe, Ultra-high-efficiency Residential Power System 3 Rd European Fuel Cell Technology Applications Conference, (2009).
[19] T. Elmer, M. Worall, S. Wu, S.B. Riffat, Emission and economic performance assessment of a solid oxide fuel cell micro-combined heat and power system in a domestic building, Appl. Therm. Eng. 90 (2015) 1–8, http://dx.doi.org/10.1016/j.applthermaleng.2015.03.078.
[20] L. Mastropasqua, S. Campanari, P. Iora, M.C. Romano, Simulation of intermediate-temperature SOFC for 60%+ efficiency distributed generation, ASME 2015 13th Int. Conf. Fuel Cell Sci. Eng. Technol, ASME, San Diego, California, 2015, , http://dx.doi.org/10.1115/FUELCELL2015-49373 V001T05A003.
[21] H. Madi, A. Lanzini, D. Papurello, S. Diethelm, C. Ludwig, M. Santarelli, et al., Solid oxide fuel cell anode degradation by the effect of hydrogen chloride in stack and single cell environments, J. Power Sources 326 (2016) 349–356, http://dx.doi.org/10.1016/j.jpowsour.2016.07.003.
[22] D. Papurello, A. Lanzini, S. Fiorilli, F. Smeacetto, R. Singh, M. Santarelli, Sulfur poisoning in Ni-anode solid oxide fuel cells (SOFCs): deactivation in single cells and a stack, Chem. Eng. J. 283 (2016) 1224–1233, http://dx.doi.org/10.1016/j.cej.2015.08.091.
[23] D. Lauinger, P. Caliandro, J. Van herle, D. Kuhn, A linear programming approach to

the optimization of residential energy systems, 7 (2016) 24–37, http://dx.doi.org/10.1016/j.est.2016.04.009.
[24] GE developing hybrid SOFC-gas engine for distributed generation, Fuel Cells Bull. 2013 (2013) 2013, http://dx.doi.org/10.1016/S1464-2859(13)70346-8.
[25] LG Fuel Cell Systems, LG fuel cell systems SOFC technology and SECA program update, 15th Annu, SECA, 2014.
[26] D. Montinaro, a. R. Contino, a. Dellai, M. Rolland, Determination of the impedance contributions in anode supported solid oxide fuel cells with (La,Sr)(Co,Fe)O3 − δ cathode, Int. J. Hydrogen Energy 39 (2014) 21638–21646, http://dx.doi.org/10.1016/j.ijhydene.2014.09.081.
[27] F. Mueller, J. Brouwer, F. Jabbari, S. Samuelsen, Dynamic simulation of an integrated solid oxide fuel cell system including current-based fuel flow control, J. Fuel Cell Sci. Technol. 3 (2006) 144, http://dx.doi.org/10.1115/1.2174063.
[28] L. Mastropasqua, S. Campanari, G. Valenti, A. Guariniello, S. Modena, F. Ghigliazza, Testing and preliminary modelling of a 2.5 kW micro-CHP SOFC unit, ASME 2016 14th Int. Conf. Fuel Cell Sci. Eng. Technol, ASME, 2016, , http://dx.doi.org/10.1115/FUELCELL2016-59327 V001T04A003.
[29] G.E.P. Box, J.S. Hunter, W.G. Hunter, Statistics for Experimenters, second ed., (2005) wi.
[30] A. Bertei, G. Arcolini, J.P. Ouweltjes, Z. Wuillemin, P. Piccardo, C. Nicolella, Physically-based deconvolution of impedance spectra: interpretation, fitting and validation of a numerical model for lanthanium strontium cobalt ferrite-based solid oxide fuel cells, Electrochim. Acta 208 (2016) 129–141, http://dx.doi.org/10.1016/j.electacta.2016.04.181.
[31] V. Sonn, A. Leonide, E. Ivers-Tiffée, Combined deconvolution and CNLS fitting approach applied on the impedance response of technical Ni/8YSZ cermet electrodes, J. Electrochem. Soc. 155 (2008) B675, http://dx.doi.org/10.1149/1.2908860.
[32] R. Yu, W. Guan, X.-D. Zhou, Probing temperature inside planar SOFC short stack, Modul. Stack Ser. Jom 69 (2017) 247–253, http://dx.doi.org/10.1007/s11837-016-2155-z.
[33] Z. Wuillemin, S. Ceschini, Y. Antonetti, C. Beetschen, S. Modena, D. Montinaro, et al., High-performance SOFC stacks tested under different reformate compositions, 11th Eur. SOFC SOE Forum, Lucerne, 2014.